Implementations of multiphysics simulation for MEMS by coupling single-physics solvers

Jian Guo
School of Mechanical Engineering,
University of Leeds, Leeds LS2 9JT, UK
E-mail: mengj@leeds.ac.uk

Osvaldo M. Querin
School of Mechanical Engineering
University of Leeds, Leeds LS2 9JT, UK
E-mail: ozz@mech-eng.leeds.ac.uk

ABSTRACT

Due to the growing demands from industries, the multiphysics simulation plays a more and more important role in the design of MEMS devices. This paper presents a fast convergence scheme which implements multiphysics simulation by coupling phenomena-specific single-physics solvers. The proposed scheme is based on the traditional staggered/relaxation approach but employs the Steffensen's acceleration technique to speed up the convergence procedure. The performance of the proposed scheme is compared with three traditional techniques: the staggered/relaxation, the multilevel Newton and the quasi-Newton methods through several examples. The results show that this scheme is promising.

1. INTRODUCTION

The rapid development of Micro-Electro-Mechanical System (MEMS) industry has growing demands for efficient, robust and easily used design tools for MEMS devices. However, the design of MEMS is a challenging task since the fundamental actuating and sensing mechanisms are always based on the interactions of multiphysics phenomena [1]. In the past two decades, these interactions were accounted by low-fidelity models. Whereas more recently, thanks to the advancement of computer powers, the utility of high-fidelity models for the design of MEMS has been widely recognized, and several tools such as FEMLAB [2] and ANSYS Multiphysics [3], also have been produced based on Finite Element (FE) techniques. Nevertheless, a desirable MEMS design tool should have the following features: 1) Account for closely-coupled multiphysics phenomena at high-fidelity level; 2) Avoid the sole usage of FE techniques because it is not always the best choice for all the physical phenomena, for example, the Boundary Element (BE) method is much more efficient than FE for electrostatic computations; 3) Utilize existing, commercially available phenomena-specific tools. Therefore, implementing multiphysics simulation for MEMS using phenomena-specific single-physics solvers is essential.

Several numerical coupling techniques have been developed for multiphysics simulation of MEMS devices. The widely used staggered/relaxation method is very convenient and easy to program, furthermore, it is a black-box based method and therefore can be easily extended to include more coupled physical phenomena without the modification on commercial single-physics solvers [4]. However, many numerical examples indicated that the staggered/relaxation method is extremely slow and sometimes fails to converge for strong coupling or nonlinear problems [5]. The Newton method can be very quick and efficient compared to the staggered/relaxation method, but it has no black-box capability and, hence, is not easy to be connected with existing field-specific analysis tools [6]. The multilevel Newton method permits the robust convergence properties of the Newton method to be realized in black-box architecture and, has been proven to be very accurate, efficient and convergent even when there is strong coupling between physical fields, but it has considerable computing loads within each iteration step [7]. Furthermore, some other techniques such as quasi-Newton method [8] also seem to be suitable for multiphysics simulations of MEMS, but have not been investigated adequately yet under the context of using phenomena-specific single-physics solvers.

The objective of this paper is to introduce a novel fast convergence scheme which implements multiphysics simulation of MEMS by coupling black-box based phenomena-specific solvers for involved physics. This scheme is based on the traditional staggered/relaxation method but employs the Steffensen's acceleration technique to speed up the convergence procedure therefore giving good convergence performance while keeping the advantages of the staggered/relaxation method.

The organization of this paper is as follows. In the next section the problem formulation of multiphysics simulation is presented, in the context of MEMS electrostatic actuators. Then section 3 provides an overview of conventional numerical coupling techniques, i.e. the staggered/relaxation, the multilevel Newton and the quasi-Newton methods. Section 4 introduces the proposed fast convergence scheme, including the principle and the implementing procedure. In section 5, this scheme is applied to several electrostatic actuator examples by coupling phenomena-specific single-physics FE/BE solvers, and the numerical results are compared with those of conventional methods reviewed in section 3. The conclusion is given in the last section.

2. MEMS ELECTROSTATIC ACTUATORS

The fundamental actuating and sensing mechanisms of MEMS devices are always based on the interactions of multiphysics phenomena. For example, the electromechanical couplings in MEMS comb drives and, the interaction between electrostatic, mechanical and fluidic fields in microresonator-based gyroscopes [9]. This multiphysics nature of MEMS devices makes the problem formulation much more complicated than the conventional single-physics problem.

MEMS family comprises large numbers of categories, among which electrostatic actuators are the most typical MEMS devices as the effect of electrostatic force is amplified in the micro-scale world. The behaviors of electrostatic actuators have been widely studied; therefore they are perfect benchmark for investigating multiphysics simulation problems.

2.1. GOVERNING EQUATIONS

The electrostatic actuator usually involves a mechanical structure which undergoes deformation when subjected to electrostatics force and conversely, the electrostatics charge

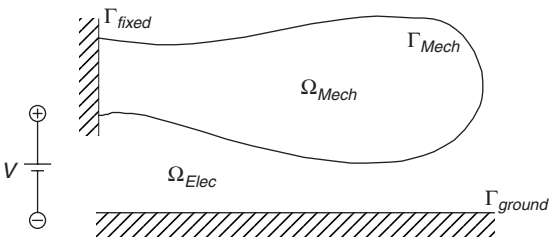

Figure 1 Schematic setup of the electrostatic actuator.

distribution is also changed due to the structural deformation. The equilibration is obtained until the mechanical and electrostatic force balance each other. A well known example of the electrostatic actuator is the MEMS parallel plate capacitor [9]. A schematic setup for electrostatic actuators is shown in Figure 1.

Generally, the involved physics in MEMS devices are described as continuous field models which couple the relevant field quantities such as mechanical, thermal, electrical, etc. in terms of a system of Partial Differential Equations (PDEs) [5]. Consider the electrostatic actuator illustrated in Figure 1, the governing equation for the mechanical displacement field can be written as a Navier-Cauchy equilibrium equation [10] of the following form:

$$\mathbf{P}+\mu\nabla^2\mathbf{u}+(\lambda+\mu)\nabla\nabla\cdot\mathbf{u}=\mathbf{0} \qquad in\ \Omega_{Mech} \tag{1}$$

with boundary conditions $\mathbf{u} = \mathbf{0}$ at Γ_{fixed}, where $\mathbf{u}$ is the structural displacement, $\mathbf{P}$ the electrostatic pressure, ∇ the vector differential operator, μ and λ are the first and second Lame parameters in terms of Young's modulus E and Poisson ratio ν as

$$\begin{cases} \mu = \dfrac{E\nu}{(1-\nu)(1-2\nu)} \\ \lambda = \dfrac{E}{2(1+\nu)} \end{cases} \tag{2}$$

The electrostatic field is described by the Laplace's equation [11]

$$-\nabla\cdot\varepsilon\nabla\varphi=0 \qquad in\ \ \Omega_{Elec} \tag{3}$$

with boundary conditions $\varphi = 0$ at Γ_{ground} and $\varphi = V$ at Γ_{fixed}, where ε is the permittivity, φ the electric potential and V the applied voltage. The electric field then yields

$$\mathbf{E}=-\nabla\varphi \tag{4}$$

and the electrostatic force acting on the surface of the structure is

$$\mathbf{P}=\left(-\varepsilon\mathbf{E}\mathbf{E}+\frac{1}{2}\varepsilon\left\|\mathbf{E}\right\|^2\mathbf{I}\right)\cdot\mathbf{n} \tag{5}$$

where $\mathbf{I}$ is the identity matrix and $\mathbf{n}$ the unit vector.

The field quantities in the electrostatic field are related with the geometry, therefore Eqns.(1)~(5) can be regarded as describing the electrostatic actuator by a system of two PDEs with two coupled field quantities, i.e. **u** and **P**.

2.2. ALTERNATIVE FORMULATIONS USING SINGLE-PHYSICS SOLVERS

Let functions R_M and R_E respectively represent the left-hand side of Eqns.(1) and (5), **u** and **P** respectively represent the state vectors of the mechanical and the electrostatic fields, the multiphysics problem of the electrostatic actuator is then formulated in a simplified form as

$$\begin{pmatrix} R_M(\mathbf{u},\mathbf{P}) \\ R_E(\mathbf{u},\mathbf{P},V) \end{pmatrix} = \mathbf{0} \tag{6}$$

A field-specific FE solver can be used to solve each PDE in Eqn.(6) for **u** or **P** provided that the state vector of another field is specified. However, by itself, a field-specific FE solver cannot solve the multiphysics problem for which the goal is to find a complete set of state vectors that simultaneously solve all equations in Eqn.(6). Therefore, this system of coupled PDEs can be solved using FE techniques only if problem-specific coupled-field elements have been implemented. Several FE-based commercial software partially have the ability of multiphysics simulation. A typical example is the Direct Coupled-Field Analysis function in ANSYS which include 20 coupled-field elements [12].

However, FE is not always the best choice for all areas of physics. For instance, if the FE method is used for both the mechanical and the electrostatic fields of the electrostatic actuator, not only the interior of the mechanical field but also the whole electric field have to be meshed, which requires a large number of nodes and the resulting system of equations will be computationally expensive to solve. While using BE for computing the electrostatic field, only surfaces are discretized and only surface quantities are computed instead of the entire domain, which is much more efficient than FE. Therefore, by using the most appropriate single-physics solvers for relevant fields, the efficiency of multiphysics simulation can be greatly improved.

Single-physics solvers, especially commercial tools, are mostly black-box based. For the simulation of the electrostatic actuator, the mechanical field-specific solvers such as ANSYS [3] and ABAQUS [13] take the electrostatic force as input and the displacement as output, and the electrostatic domain-specific solvers such as FASTCAP [14] export surface charge distribution and the induced electrostatic force according to the deformed geometry and the applied voltage, as illustrated in Figure 2. In order to utilize these solvers, the two equations in Eqn.(6) are re-formulated as

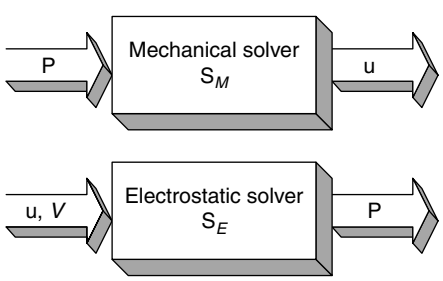

Figure 2 Field-specific solvers.

$$\begin{cases} \mathbf{u} = \mathrm{S}_M(\mathbf{P}) \\ \mathbf{P} = \mathrm{S}_E(\mathbf{u}, V) \end{cases} \tag{7}$$

where functions S_M and S_E respectively represent the black-box based FE solver for the mechanical field and the BE solver for the electrostatic field, $\mathbf{P}$ and $\mathbf{u}$,V are the input/output for these solvers. The system in Eqn.(6) is then transformed to

$$\mathrm{F}(\mathbf{u}, \mathbf{P}) = \begin{pmatrix} \mathbf{u} - \mathrm{S}_M(\mathbf{P}) \\ \mathbf{P} - \mathrm{S}_E(\mathbf{u}, V) \end{pmatrix} = \mathbf{0} \tag{8}$$

where function F is defined as the system residual.

Although Eqns.(6) and (8) are both general formulations of electrostatic actuator problems, there are still slight differences between them. The previous is a system of PDEs, while the latter is a system of implicit functions defined by the previous. According to the Implicit Function Theorem, the latter exists only if the previous has a solution, which means that a solution of Eqn.(8) must also be a solution of Eqn.(6), while the other direction may not necessarily be true. However, the multiphysics problem is still solvable by using either the original formulation in Eqn.(6) or the one in Eqn.(8). In this sense, these two formulations are equivalent. In this paper, only the latter one, i.e. Eqn.(8) is used because it provides a mechanism for conveniently connecting together a variety of commercially available single-physics solvers to form *black-box* property [1] only through the input/output relationship without any modification.

3. COVENTIONAL COUPLING APPROACHES

No matter which formulation is used, the multiphysics problem is usually regarded as a system of nonlinear equations which can be solved by many approaches. In this section, three conventional numerical coupling techniques, i.e. the staggered/relaxation, the multilevel Newton and the quasi-Newton methods, will be briefly reviewed in the context of the electrostatic actuator problem described in Eqn.(8).

3.1. STAGGERED/RELAXATION METHOD

The simplest but also the most popular coupling approach for multiphysics simulations is the staggered/relaxation method [4] which is based on the nonlinear Gauss-Seidel algorithm [16] and does not require calculations of derivatives.

As illustrated in Figure 3, for the system in Eqn.(8), this approach adopts the Gauss-Seidel algorithm to iteratively computes the sequential substitution as

$$\begin{cases} \mathbf{P}^{(k+1)} = \mathrm{S}_E(\mathbf{u}^{(k)}, V) \\ \mathbf{u}^{(k+1)} = \mathrm{S}_M(\mathbf{P}^{(k+1)}) \end{cases} \tag{9}$$

until the difference between two consecutive iterations is less than a small value. From engineering perspective, this procedure can be summarized as sequentially applying results from one single-physics solver as loads of the next one, therefore this approach is also called the sequential method in some literatures [12].

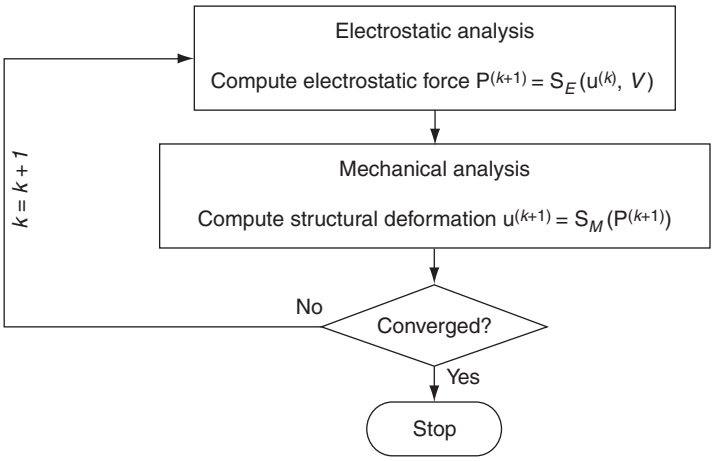

Figure 3 The staggered/relaxation method.

3.2. MULTILEVEL NEWTON METHOD

A more robust approach is the multilevel Newton method [7]. It's based on the Newton method which is used to solve a system of nonlinear equations [8].

The multilevel Newton method has a two-level nested loop structure as shown in Figure 4. The outer loop solves Eqn. for $[\mathbf{u},\mathbf{P}]^T$ by a Newton iterative procedure

$$\begin{bmatrix} \mathbf{u}^{(k+1)} \\ \mathbf{P}^{(k+1)} \end{bmatrix} = \begin{bmatrix} \mathbf{u}^{(k)} \\ \mathbf{P}^{(k)} \end{bmatrix} + \begin{bmatrix} \Delta\mathbf{u} \\ \Delta\mathbf{P} \end{bmatrix} \tag{10}$$

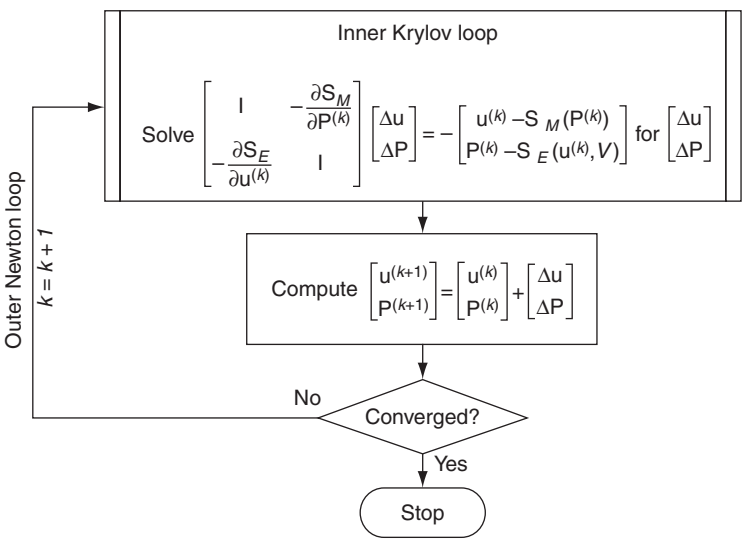

Figure 4 The multilevel Newton method.

while the inner loop calculate the Newton step-length $[\Delta\mathbf{u}, \Delta\mathbf{P}]^T$ by solving the formed linear system

$$\mathrm{F}'(\mathbf{u}^{(k)}, \mathbf{P}^{(k)}) \cdot \begin{bmatrix} \Delta\mathbf{u} \\ \Delta\mathbf{P} \end{bmatrix} = -\mathrm{F}(\mathbf{u}^{(k)}, \mathbf{P}^{(k)}) \tag{11}$$

for $[\Delta\mathbf{u}, \Delta\mathbf{P}]^T$ during each outer Newton iteration. Note here k is the outer Newton iteration index and kept fixed when inner iteration proceeds.

The key step of the outer loop is to compute $[\Delta\mathbf{u}, \Delta\mathbf{P}]^T$ for each outer iteration, but since the system Jacobian is

$$\mathrm{F}'(\mathbf{u}^{(k)}, \mathbf{P}^{(k)}) = \begin{bmatrix} \mathbf{I} & -\dfrac{\partial \mathrm{S}_M}{\partial \mathbf{P}^{(k)}} \\ -\dfrac{\partial \mathrm{S}_E}{\partial \mathbf{u}^{(k)}} & \mathbf{I} \end{bmatrix} \tag{12}$$

it will be very difficult to obtain $[\Delta\mathbf{u}, \Delta\mathbf{P}]^T$ directly through Eqn.(11) because the off-diagonal derivatives, i.e. $\partial\mathbf{S}_M/\partial\mathbf{P}^{(k)}$ and $\partial\mathbf{S}_E/\partial\mathbf{u}^{(k)}$, may not be available explicitly, or are time consuming to be computed even if be available through finite difference. Therefore a variety of Krylov-subspace methods, here Generalized Minimal RESidual (GMRES) [17], is used to solve Eqn. for $[\Delta\mathbf{u}, \Delta\mathbf{P}]^T$ by the inner loop.

During the solution procedure, GMRES requires the action of the Jacobian only in the form of matrix-vector products, which may be approximated by first order finite difference as

$$\mathrm{F}'(\mathbf{u}^{(k)}, \mathbf{P}^{(k)}) \cdot \begin{bmatrix} \mathbf{r}_{\mathbf{u}}{}^{(j)} \\ \mathbf{r}_{\mathbf{P}}{}^{(j)} \end{bmatrix} = \frac{\mathrm{F}(\mathbf{u}^{(k)} + \theta\mathbf{r}_{\mathbf{u}}{}^{(j)}, \mathbf{P}^{(k)} + \theta\mathbf{r}_{\mathbf{P}}{}^{(j)}) - \mathrm{F}(\mathbf{u}^{(k)}, \mathbf{P}^{(k)})}{\theta} \tag{13}$$

where $[\mathbf{r}_{\mathbf{u}}{}^{(j)}, \mathbf{r}_{\mathbf{P}}{}^{(j)}]^T$ is the residual of the jth inner iteration, and θ is a small perturbation defined as a matrix-free parameter. Since only matrix-vector products are required instead of a matrix, GMRES is usually regarded as the matrix-free method [18]. For more details of GMRES and other Krylov-subspace methods please refer to [17] and [18].

3.3. QUASI-NEWTON METHODS

Quasi-Newton methods are standard approaches for solving a system of nonlinear equations, however, their application on black-box based formulation has not been reported before.

Like other Newton type methods, quasi-Newton methods also use the Newton iterative procedure to solve Eqn.(8) for $[\mathbf{u},\mathbf{P}]^T$ as:

$$\begin{bmatrix} \mathbf{u}^{(k+1)} \\ \mathbf{P}^{(k+1)} \end{bmatrix} = \begin{bmatrix} \mathbf{u}^{(k)} \\ \mathbf{P}^{(k)} \end{bmatrix} - \left[\mathrm{F}'(\mathbf{u}^{(k)}, \mathbf{P}^{(k)})\right]^{-1} \cdot \mathrm{F}(\mathbf{u}^{(k)}, \mathbf{P}^{(k)}) \tag{14}$$

Since the system Jacobian $\mathrm{F}'(\mathbf{u}^{(k)},\mathbf{P}^{(k)})$ is usually difficult to be computed, it (or its inverse $[\mathrm{F}'(\mathbf{u}^{(k)},\mathbf{P}^{(k)})]^{-1}$) can be approximated. According to the way of approximating the Jacobian, quasi-Newton methods have many varieties. In this paper we adopt the most popular Broyden's method [8] which approximates the Jacobian and update the approximation when the nonlinear iteration progresses.

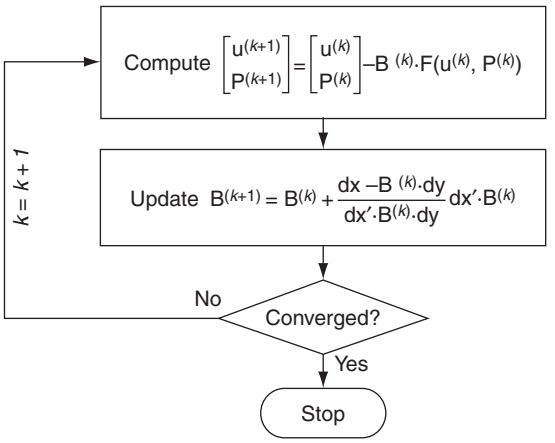

Figure 5 Broyden's method.

Broyden's method is illustrated in Figure 5. Assume $[\mathbf{u}^{(k)},\mathbf{P}^{(k)}]^T$ and $\mathbf{B}^{(k)}$ are the current approximations of the true solution $[\mathbf{u}^*,\mathbf{P}^*]^T$ and the Jacobian's inverse $[F'(\mathbf{u}^{(k)},\mathbf{P}^{(k)})]^{-1}$ respectively, then the kth nonlinear Newton iteration is

$$\begin{bmatrix} \mathbf{u}^{(k+1)} \\ \mathbf{P}^{(k+1)} \end{bmatrix} = \begin{bmatrix} \mathbf{u}^{(k)} \\ \mathbf{P}^{(k)} \end{bmatrix} - \mathbf{B}^{(k)} \cdot \mathrm{F}(\mathbf{u}^{(k)}, \mathbf{P}^{(k)}) \tag{15}$$

After the computation of $[\mathbf{u}^{(k+1)},\mathbf{P}^{(k+1)}]^T$, $\mathbf{B}^{(k)}$ is updated to form $\mathbf{B}^{(k+1)}$ using the Broyden update as

$$\mathbf{B}^{(k+1)} = \mathbf{B}^{(k)} + \frac{\mathbf{dx} - \mathbf{B}^{(k)} \cdot \mathbf{dy}}{\mathbf{dx}' \cdot \mathbf{B}^{(k)} \cdot \mathbf{dy}} \mathbf{dx}' \cdot \mathbf{B}^{(k)} \tag{16}$$

where

$$\begin{cases} \mathbf{dy} = \mathrm{F}(\mathbf{u}^{(k+1)}, \mathbf{P}^{(k+1)}) - \mathrm{F}(\mathbf{u}^{(k)}, \mathbf{P}^{(k)}) \\ \mathbf{dx} = \begin{bmatrix} \mathbf{u}^{(k+1)} \\ \mathbf{P}^{(k+1)} \end{bmatrix} - \begin{bmatrix} \mathbf{u}^{(k)} \\ \mathbf{P}^{(k)} \end{bmatrix} = -\mathbf{B}^{(k)} \cdot \mathrm{F}(\mathbf{u}^{(k)}, \mathbf{P}^{(k)}) \end{cases} \tag{17}$$

4. RELAXATION WITH STEFFENSEN'S ACCELERATION SCHEME

The staggered/relaxation method is easy to implement for multiphysics problems. However, it converges very slowly and sometimes fails to converge for tightly coupled or highly nonlinear problems [6]. This section presents a novel fast convergence scheme which is based on the staggered/relaxation method but improved by the Steffensen's acceleration procedure. Therefore, this scheme does not suffer from the drawbacks of the staggered/relaxation method.

4.1. PRINCIPLE

For MEMS electrostatic actuator problems studied in this paper, there exist two phenomena-specific spatial domains, i.e. the structural domain and the electrostatic domain. These two domains don't overlap and interact only through the shared boundary (the electrostatic-structure interface Γ_{Mech} in Figure 1). Since one phenomena-specific single-physics solver is used in each domain, the key issues involved in the proposed scheme are the coupling algorithm and the data exchange between two solvers.

4.1.1. Coupling Algorithm

The coupling algorithm is the numerical treatment of the coupling mechanisms among involved physics, which determines when coupling data is transferred and results in different coupled procedures. Consider the electrostatic actuator problem in Eqn.(8). Since the staggered/relaxation method is used, the *k*th iteration has already been formulated in Eqn.(9). Insert the first sub-equation of Eqn.(9) into the second one and yield

$$\mathbf{u}^{(k+1)} = \mathrm{S}_M(\mathrm{S}_E(\mathbf{u}^{(k)})) \tag{18}$$

Meanwhile, assume that $[\mathbf{u}^*,\mathbf{P}^*]^T$ is the true solution of Eqn.(8), then $\mathbf{u}^*$ and $\mathbf{P}^*$ must satisfy Eqn.(7), i.e.

$$\begin{cases} \mathbf{u}^* = \mathrm{S}_M(\mathbf{P}^*) \\ \mathbf{P}^* = \mathrm{S}_E(\mathbf{u}^*, V) \end{cases} \tag{19}$$

Therefore obtain

$$\mathbf{u}^* = \mathrm{S}_M(\mathrm{S}_E(\mathbf{u}^*)) \tag{20}$$

According to Fixed-Point Theorem [19], Eqn.(18) and (20) both imply that there exists a fixed-point problem

$$\mathbf{u} = \mathrm{g}_M(\mathbf{u}) \tag{21}$$

where g_M denotes the fixed-point mapping from $\mathbf{u}^{(k)}$ to $\mathbf{u}^{(k+1)}$ and may be nonlinear. Furthermore, the true solution $\mathbf{u}^*$ is also called a fixed-point of the mapping g_M and can be approximated by the fixed-point iterative procedure

$$\mathbf{u}^{(k+1)} = \mathrm{g}_M(\mathbf{u}^{(k)}) \tag{22}$$

which is another formulation of Eqn.(18).

Since $\mathbf{u}^{(k)}$ is an approximation of the true solution $\mathbf{u}^*$, according to the Mean Value Theorem [23], $\mathbf{u}^*$ can be expanded at $\mathbf{u}^{(k)}$ as

$$\begin{aligned} \mathbf{u}^* &= \mathrm{g}_M(\mathbf{u}^*) \\ &= \mathrm{g}_M(\mathbf{u}^{(k)}) + \mathrm{g}_M{}'(\xi)\cdot(\mathbf{u}^* - \mathbf{u}^{(k)}) \\ &= \mathbf{u}^{(k+1)} + \mathrm{g}_M{}'(\xi)\cdot(\mathbf{u}^* - \mathbf{u}^{(k)}) \end{aligned} \tag{23}$$

where ξ is an arbitrary value between $\mathbf{u}^*$ and $\mathbf{u}^{(k)}$, and $\mathrm{g}_M{}'(\xi)$ can be approximated by finite difference as

$$\begin{aligned} g_M'(\xi) &\approx \frac{g_M(\mathbf{u}^{(k)}) - g_M(\mathbf{u}^{(k-1)})}{\mathbf{u}^{(k)} - \mathbf{u}^{(k-1)}} \\ &= \frac{\mathbf{u}^{(k+1)} - \mathbf{u}^{(k)}}{\mathbf{u}^{(k)} - \mathbf{u}^{(k-1)}} \end{aligned} \tag{24}$$

Insert Eqn.(24) into (23) and extract $\mathbf{u}^*$ then obtain

$$\mathbf{u}^* \approx \mathbf{u}^{(k-1)} - \frac{\left[\mathbf{u}^{(k)} - \mathbf{u}^{(k-1)}\right]^2}{\mathbf{u}^{(k+1)} - 2\mathbf{u}^{(k)} + \mathbf{u}^{(k-1)}} \tag{25}$$

Equation (25) leads to an iterative procedure for computing $\mathbf{u}^*$ as

$$\begin{aligned} \mathbf{u}^{(k+1)} &= \mathbf{u}^{(k)} - \frac{\left[g_M(\mathbf{u}^{(k)}) - \mathbf{u}^{(k)}\right]^2}{g_M(g_M(\mathbf{u}^{(k)})) - 2g_M(\mathbf{u}^{(k)}) + \mathbf{u}^{(k)}} \\ &= \mathbf{u}^{(k)} - \frac{\left[\mathbf{y}_M - \mathbf{u}^{(k)}\right]^2}{\mathbf{z}_M - 2\mathbf{y}_M + \mathbf{u}^{(k)}} \end{aligned} \tag{26}$$

Note Eqn.(26) produces a new sequence $\{\mathbf{u}^{(k)}\}$ which is different from the one in Eqn.(25), and $\mathbf{P}^*$ also can be computed in a similar way. Since $\mathbf{y}_M$ and $\mathbf{z}_M$ are obtained through the nonlinear Gauss-Seidel algorithm in Eqn.(9), the iterative procedure in Eqn.(26) can be regarded as accelerating the convergence of Gauss-Seidel staggered/relaxation, which is similar with the fixed-point Steffensen's acceleration [16]. Therefore, this fast convergence algorithm is referred by us as Relaxation with Steffensen's Acceleration (RSA).

Since the RSA scheme is based on the staggered/relaxation method, it has some relationships with the latter. Recall Eqn.(18)-(22), it has been proved that the nonlinear Gauss-Seidel procedure in Eqn.(18) or (22) is the fixed-point iteration, g_M and g_E are the fixed-point mapping and the true solution $\mathbf{u}^*$,$\mathbf{P}^*$ is the fixed-point. Assume that $\mathbf{u}$,$\mathbf{P}$ are respectively in the neighborhood of $\mathbf{u}^*$ and $\mathbf{P}^*$, according to the Fixed-Point Theorem, the condition for convergence of the staggered/relaxation method is

$$\left\| g_M'(\mathbf{u}) \right\| \le L, \left\| g_E'(\mathbf{P}) \right\| \le L \tag{27}$$

where the constant $L \in (0,1)$.

Compare the RSA iteration in Eqn.(26) with the staggered/relaxation iteration in Eqn.(22), it can be found that the RSA procedure is virtually the fixed-point Steffensen's acceleration applied on the nonlinear Gauss-Seidel procedure. Therefore, in terms of the Steffensen's Acceleration Theorem [16,20], the condition for convergence of the RSA scheme is

$$\left\| g_M'(\mathbf{u}) \right\| \ne 1, \left\| g_E'(\mathbf{P}) \right\| \ne 1 \tag{28}$$

The convergence condition in Eqn.(28) is much looser than that in Eqn.. If Eqn.(27) is satisfied, then Eqn.(27) must also be satisfied without doubt. And even if Eqn.(27) isn't satisfied, i.e. $\|g_M'(\mathbf{u})\| > L$ or $\|g_E'(\mathbf{P})\| > L$, Eqn.(28) may still exist. This fact indicates that the

RSA scheme has the ability to speed up the staggered/relaxation method when the latter converges, and sometimes is still converging even if the latter diverges. This is an important advantage of the RSA scheme over the conventional staggered/relaxation method. However, the RSA scheme may experience some numerical instabilities when it approaches the true solution because both the numerator and the denominator in Eqn.(26) are close to zero at the same time.

4.1.2. Data Exchange

Due to the numerical discretizations in both structural and electrostatic domains, the data generated respectively by FE and BE solvers are distributed on different meshes. Therefore the data exchange within the electrostatic actuator problem is an important issue that must be accounted. Although in this paper this issue is solved using standard techniques, some details still need to be addressed for completeness.

In this paper, the structural domain is discretized by standard FE techniques. Applying the FE formulation to Eqn. leads to the well-known matrix equation for the structural quantities

$$\mathbf{M}\ddot{\mathbf{u}} + \mathbf{C}\dot{\mathbf{u}} + \mathbf{K}\mathbf{u} - \mathbf{P} = \mathbf{0} \tag{29}$$

where m is the number of discretization nodes, $\mathbf{M} \in \mathbb{R}^{3m\times 3m}$ the mass matrix, $\mathbf{C} \in \mathbb{R}^{3m\times 3m}$ the damping matrix, $\mathbf{K} \in \mathbb{R}^{3m\times 3m}$ the stiffness matrix, $\mathbf{P} \in \mathbb{R}^{3m\times 3m}$ the force vector, $\ddot{\mathbf{u}} \in \mathbb{R}^{3m}$ nodal accelerations, $\dot{\mathbf{u}} \in \mathbb{R}^{3m}$ nodal velocities and $\mathbf{u} \in \mathbb{R}^{3m}$ nodal displacements.

For the electrostatic domain, the only interested quantities are values at boundaries rather than those inside the domain, thus only the surface mesh of the electrostatic domain has to be created and only the geometry of this surface mesh (at the electrostatic-structure interface) needs to be updated when the structure changes shape. The BE discretization of Eqn.(3) yields

$$\mathbf{H}\varphi = \mathbf{G}\dot{\varphi} \tag{30}$$

where n is the number of discretization nodes, $\mathbf{H},\mathbf{G} \in \mathbb{R}^{n\times n}$ boundary element matrices, φ the nodal vector of the scalar electric potential and $\dot{\varphi}$ the nodal vector of the normal derivatives of the scalar electric potential.

As mentioned in section 2, **P** in Eqn.(29) relates to φ in Eqn.(30), while the two boundary element matrices **H** and **G** in Eqn.(30) relate to structural displacement **u** in Eqn.(29), therefore the FE/BE domains are two-way coupled through the coupling data defined on overlapped meshes at the shared boundary. However from implementation perspective, since both the structural and the electrostatic models are discretized in a physically different manner, they do not match at the boundary. This is called "non-matching" and means that the coupling data do not share the same nodes at their interface.

In the electrostatic actuator problem, the data exchange is relative simple because it is limited to the boundary conditions on the interface, i.e. the electrostatic pressures given by the BE solver are applied to structural nodes on the interface, and the nodal displacements of the interface are computed in the FE solver and transferred to BE mesh. Electrostatic pressures are adapted to the element sizes to preserve the integral and usually conserve quantities, which implies that the total pressures must balance on both sides of the interface and, therefore, a conservative interpolation is required [12]. For a conservative interpolation it is better to have a fine BE mesh and a coarse FE mesh than the converse, see Figure 6. Then each BE node $S_j \in \Gamma_{BE}$ for $j = 1,...,n$, maps onto the "partner" finite element by searching the closest structural element $\Omega_{FE}^{(e)} \in \Gamma_{FE}$ on the FE mesh (as shown in Figure 6). Since fixed meshes are used, this mapping procedure is performed only once during the initialization

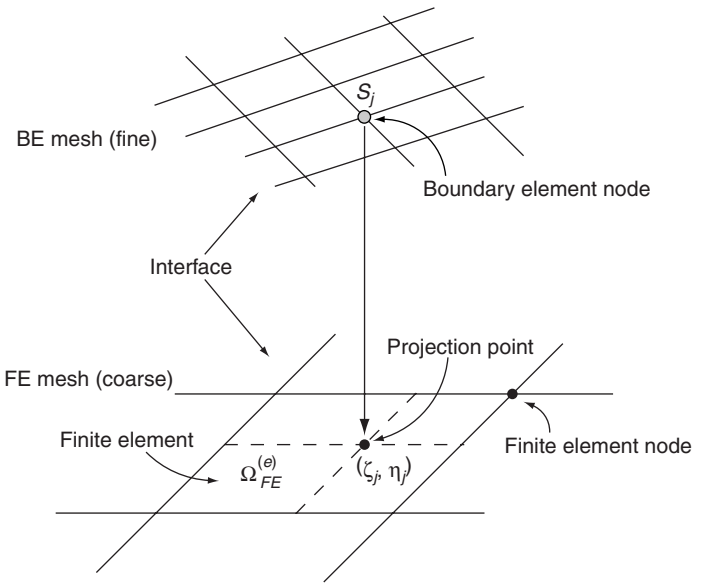

Figure 6 Data exchange.

phase. Thereafter, the FE structural load is interpolated using a conservative load projection method proposed by Farhat et. al. [21] as

$$P_{FEi} = \sum_{j=1}^{j_e} P_{BEj} N_i(\zeta_j, \eta_j) \tag{31}$$

where P_{FEi} and N_i respectively denote the structural load and finite element shape function associated with node i of element $\Omega_{FE}^{(e)}$, j_e is the total number of BE nodes associated with element $\Omega_{FE}^{(e)}$, ζ_j, η_j the local coordinates of the BE node S_j in $\Omega_{FE}^{(e)}$ and, P_{BEj} the BE nodal load.

On the other hand, transferring nodal displacements from coarser FE mesh to finer BE mesh is typically a non-conservative interpolation. Thus BE nodes still map onto closest FE elements and nodal displacements of BE nodes are interpolated by

$$u_{BEj} = \sum_{i=1}^{i_e} N_i(\zeta_j, \eta_j) u_{FEi} \tag{32}$$

where u_{BEj} for $j=1,...,je$ is the nodal displacements of BE nodes associated with element $\Omega_{FE}^{(e)}$, i_e the number of FE nodes belonging to $\Omega_{FE}^{(e)}$ and u_{FEi} the FE nodal displacements of $\Omega_{FE}^{(e)}$. Further details on data exchange have beyond the scope of this paper and can be referred to [12,21].

4.2. METHODOLOGY

The implementation of the RSA scheme consists of three main phases, i.e. pre-processing, coupling (iteration) and post-processing, as illustrated in Figure 7(a). The details of these phases are explained below, in the context of electrostatic actuator problems.

4.2.1. Pre-processing

As shown in Figure 7(b), the purpose of the pre-processing is to prepare essential information for subsequent FE/BE computation and coupling data exchange. Like standard FE or BE method, the first step of the pre-processing is to discretize the structural and electrostatic domains respectively using FE and BE techniques described in Eqns.(29) and (30), thus results in initial FE and BE meshes.

Then based on meshes topological and nodal information, the mapping relationship between FE and BE meshes are established by: 1) performing a loop over all FE elements belonging to the interface and searching for each element the involved BE nodes projections and, 2) determining the local coordinates of the BE node concerning its "partner" finite element.

Thereafter, the last step of the pre-processing phase is to set up the initial conditions respectively for FE and BE solvers. Here the conditions include the initial nodal displacements on FE mesh and electrostatic pressures on BE mesh.

4.2.2. Coupling

After pre-processing, the RSA scheme proceeds to its kernel: coupling. This is an iterative procedure comprises three main steps, as shown in Figure 7(c).

The first step, called *Relaxation Procedure I*, uses the nonlinear Gauss-Seidel algorithm in Eqn.(9) only once to solve the whole system by sequentially calling FE and BE solvers. In other words, the electrostatic pressure computed in last iteration (i.e. $\mathbf{P}_{BE}^{(k)}$) is transferred to the FE mesh and interpolated at the structural interface nodes according to Eqn.(31), the resulting pressure $\mathbf{P}_{FE}^{(k)}$ are used as load for structural FE analysis to obtain the structural displacement $\mathbf{y}_{M\_FE}$. As the structure deforms, the displacement of the electrostatic nodes at the interface is obtained by interpolating on FE mesh according to Eqn.(32) and then used as the boundary condition for electrostatic field calculation. Once this step finishes, two intermediate variables, i.e. displacement $\mathbf{y}_{M\_FE}$ and electrostatic pressure $\mathbf{y}_{E\_BE}$ are obtained, which correspond to $\mathbf{y}_M$ and $\mathbf{y}_E$ in Eqn.(26).

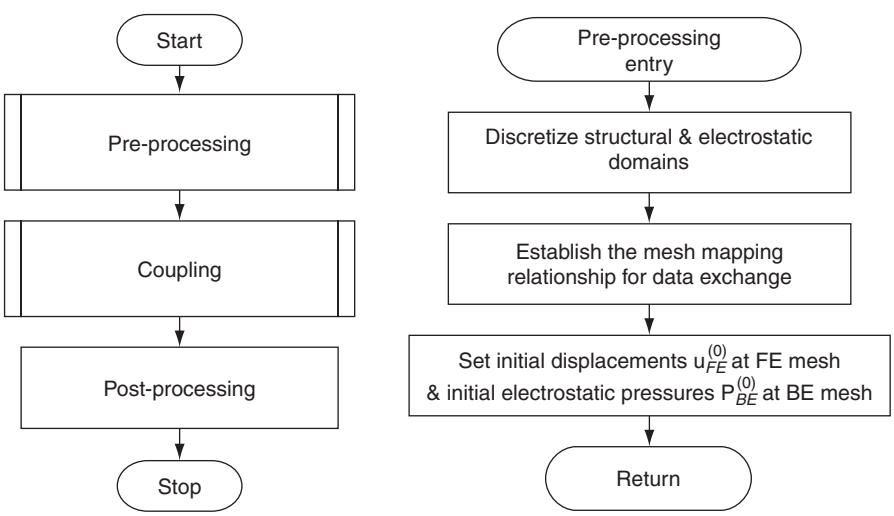

(a) Schematic of the RSA scheme (b) Pre-processing procedure

Figure 7 *(Continued).*

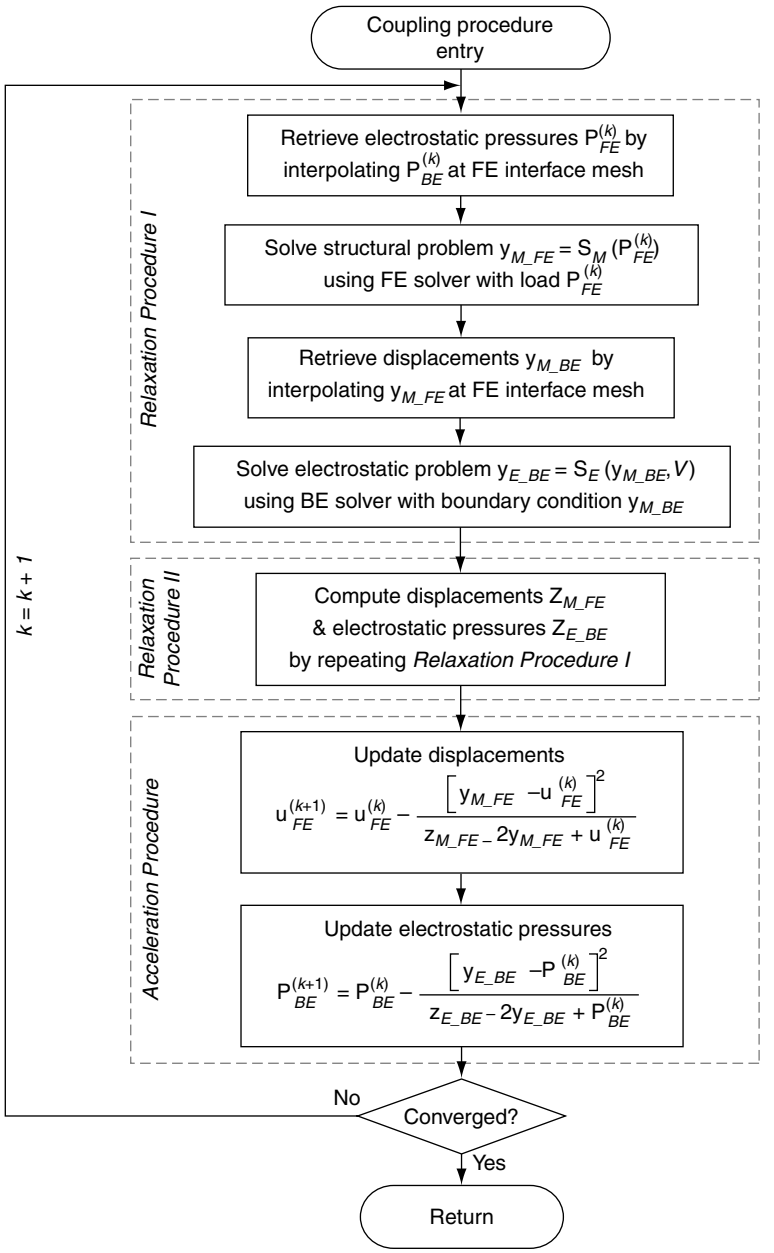

(c) Coupling procedure

Figure 7 The RSA scheme.

The second step, i.e. *Relaxation Procedure II*, repeats step one with slight differences. It transfers the intermediate value of electrostatic pressure $\mathbf{y}_E$ instead of $\mathbf{P}_{BE}^{(k)}$ to FE solver and, therefore, produces another two intermediate variables displacement $\mathbf{z}_{M\_FE}$ and electrostatic pressure $\mathbf{z}_{E\_BE}$, which correspond to $\mathbf{z}_M$ and $\mathbf{z}_E$ in Eqn.(26).

Thereafter the third step, called *Acceleration Procedure*, adapts the Steffensen's acceleration technique in Eqn.(26) to compute structural displacement $\mathbf{u}_{FE}^{(k+1)}$ based on the

intermediate variables $\mathbf{y}_{M\_FE}$, $\mathbf{z}_{M\_FE}$ and previous iteration result $\mathbf{u}_{FE}^{(k)}$ as well as electrostatic pressure $\mathbf{P}_{BF}^{(k+1)}$ based on $\mathbf{y}_{E\_BE}$, $\mathbf{z}_{E\_BE}$ and $\mathrm{P}_{BE}^{(k)}$.

Above three steps are implemented successively, until a pre-defined termination condition is satisfied.

4.2.3. Post-processing

When the iteration in the coupling procedure stops, the resulting displacement **u** and pressure **P** as well as their iterative histories and other information are retrieved and output for storage or display. This is a very standard procedure and will not be introduced furthermore.

The implementing of the RSA scheme is relative simple and easy for programming, which is the most important advantage of it. It also can be found that during the coupling phase, each iteration requires two successive relaxation procedures which are involved in the staggered/relaxation method. Since these procedures are the most time-consuming parts in the RSA scheme, the computational cost of every RSA iteration is almost as twice as that of the relaxation iteration. However, as will be shown in section 5, the RSA scheme needs much less iterations to achieve convergence for tightly-coupled problems, therefore the total cost is relatively lower even if compared with the multilevel Newton and the quasi-Newton methods. Furthermore, as illustrated in section 5 and proved in this section, the RSA scheme has looser convergence conditions than the staggered/relaxation method, therefore it may converge even if the latter fails.

5. NUMERICAL RESULTS

In this section, three electrostatic actuator examples including the MEMS parallel plate capacitor, the cantilever micro-beam and the cross bars, will be presented to compare the RSA scheme with other three conventional methods introduced in previous section. In all these examples, the mechanical computations are implemented using FE solver, and the electrostatic calculations are executed by BE solver.

5.1. MEMS PARALLEL PLATE CAPACITOR

The MEMS parallel plate capacitor is the simplest transducer whose behavior can be determined analytically, so it is the most appropriate benchmark to verify different approaches for multiphysics simulations.

The capacitor studied here consists of a movable top plate positioned $g_0 = 1\mu m$ above a fixed bottom one with the area of $A_p = 100\mu m^2$ each, and an elastic beam which has the Young's modulus $E = 1GPa$ and a 3-D dimension of $L \times A_b = 81\mu m \times 2\mu m$ [22], as in Figure 8. The top end of the beam is fixed, and the other end is attached to the movable top plate. If a voltage V is applied to the capacitor, charges with different polarities will be distributed on the surfaces of two plates. Hence, the induced electrostatic force will pull the top plate down and stretch the attached beam, until reaches a position where the mechanical force due to the beam stretching can balance the electrostatic force. As the applied voltage increases, the top plate approaches the bottom and eventually touches it at a certain applied voltage V_{PI} which is called the pull-in voltage.

According to Cai et.al. [22], the behavior of the top plate is given by

$$\frac{\varepsilon A_p V^2}{2\left(g_0 - u\right)^2} = \frac{EA_b}{L} u \tag{33}$$

where u is the displacement of the top plate and ε the pemittivity. The pull-in voltage was estimated by Senturia [9] as

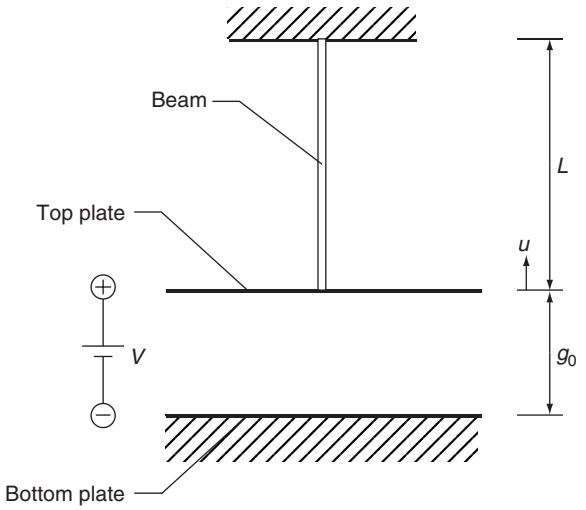

Figure 8 MEMS parallel plate capacitor.

$$V_{PI} = \sqrt{\frac{8EA_b g_0^3}{27\varepsilon A_p L}} = 90.90\text{V} \tag{34}$$

For the purpose of demonstration, the beam is discretized into 81 beam elements for FE analysis and both plates are discretized into 100 4-node elements for BE analysis. The displacements of the top plate obtained through the RSA scheme as well as other three

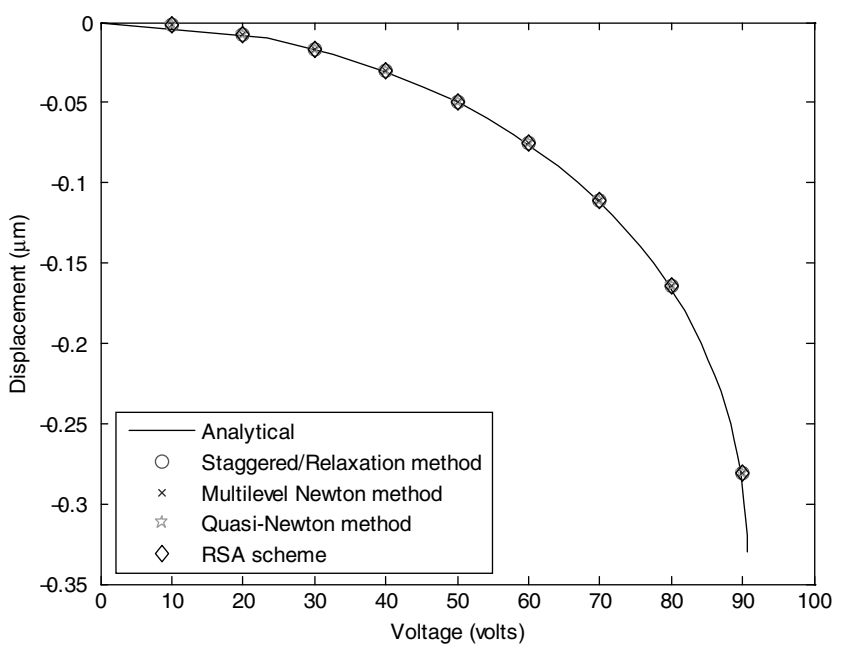

Figure 9 The displacements of the top plate for different voltages.

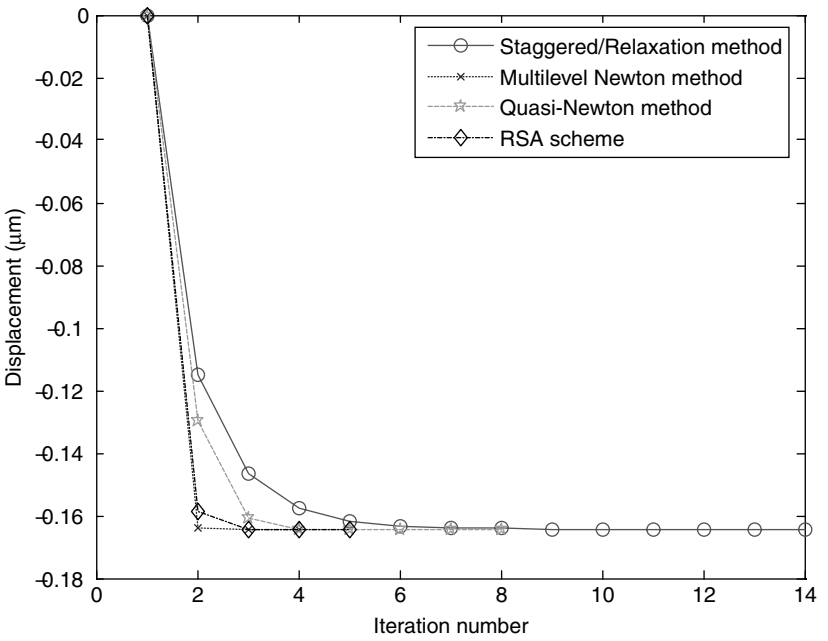

(a) Applied voltage at 80V (global view)

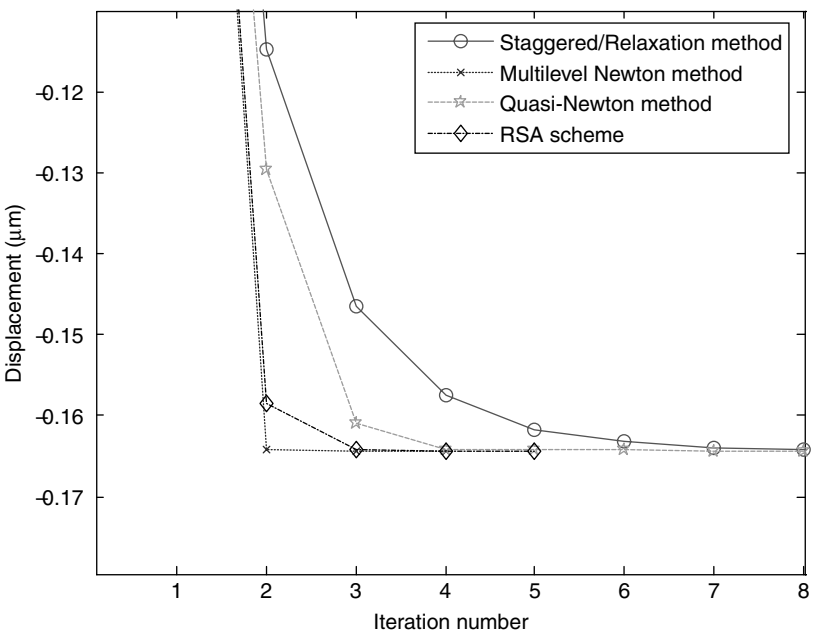

(b) Applied voltage at 80V (local enlargement)

Figure 10 *(Continued).*

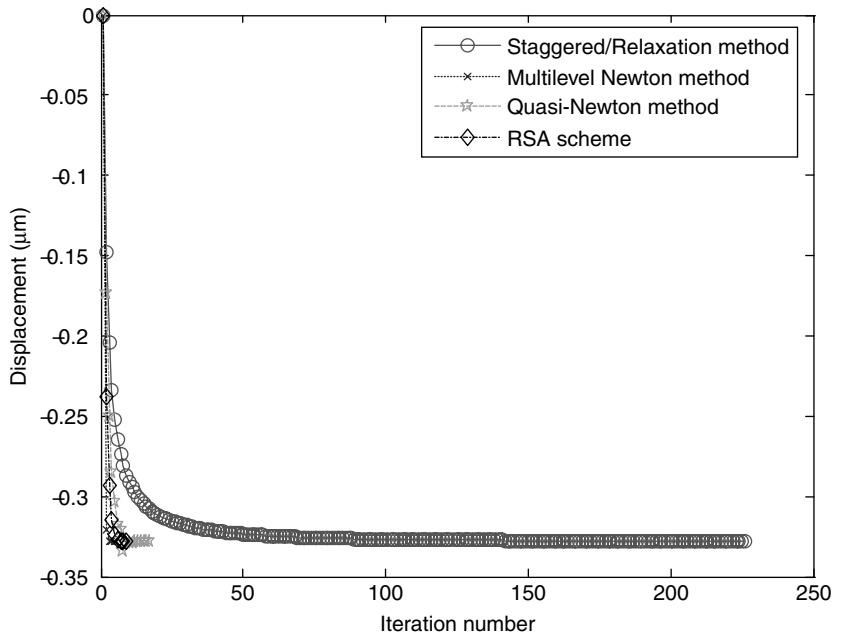

(c) Applied voltage at 90.89V (global view)

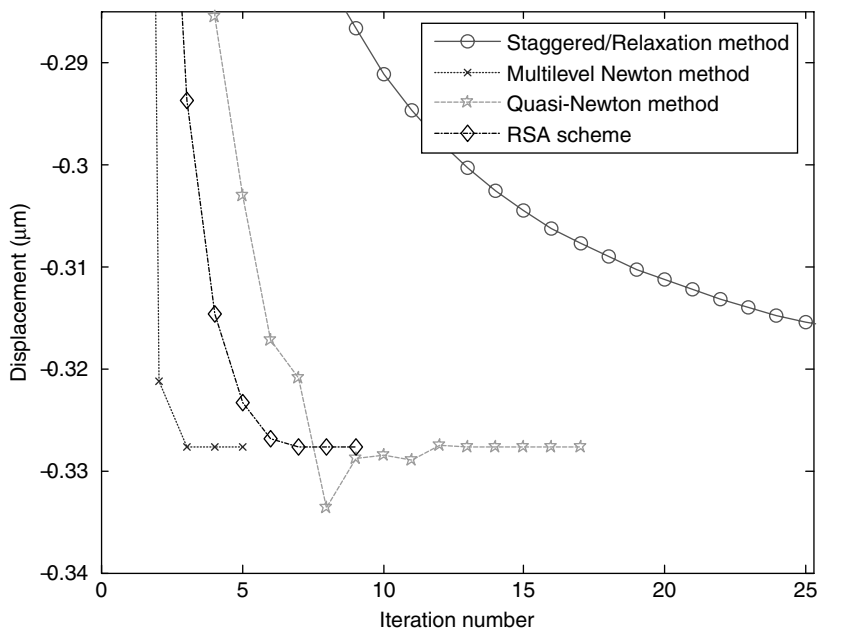

(d) Applied voltage at 90.89V (local enlargement)

Figure 10 Convergence histories for parallel plate capacitor example.

Table 1 Performances for parallel plate capacitor example

Voltage (V)	Function evaluations				CPU time (s)			
	Staggered/ relaxation	Multilevel Newton	Quasi-Newton	RSA	Staggered/ relaxation	Multilevel Newton	Quasi-Newton	RSA
10	4	10	5	6	2	14	10	3
30	5	12	5	6	4	17	11	4
50	7	14	6	8	5	16	12	6
70	11	14	6	8	10	20	12	6
80	14	16	8	10	13	20	16	8
90	42	18	11	12	33	26	20	11
90.8	99	20	15	16	54	32	25	15
90.85	128	23	17	16	67	40	28	16
90.89	226	20	17	18	119	36	30	17
90.90	Failed	Failed	Failed	Failed	N/A	N/A	N/A	N/A

methods are compared with the analytical values, as shown in Figure 9. The simulation results overlap each other and are all in good agreements with the analytical values verifying the accuracy of these four methods.

The convergence histories of the four methods are compared in Figure 10. As shown in Figure 10(a) and (b), when the applied voltage is 80V, all the four methods converge to the same value with similar iteration numbers although the staggered/relaxation and the quasi-Newton methods are a little slower. But when the voltage of 90.89V (i.e. just before pull-in) is applied, as in Figure 10(c) and (d), the staggered/relaxation method converges much more slowly, while other three methods converge rapidly. Note here the needed iterations for the quasi-Newton method is 17, the RSA scheme is 9, and the multilevel-Newton is only 5.

The performances of the four methods for different applied voltages are summarized in Table 1. All these methods converge until the pull-in voltage 90.90V verifying their accuracy. Furthermore, as the applied voltage increases, the required iterations and CPU time for the staggered/relaxation method also increases rapidly, while other three methods increase relatively smoothly. It also should be noticed that although the multilevel Newton method takes fewer outer iterations than other three methods for high voltages, it requires more function evaluations and CPU time than the quasi-Newton and the RSA methods due to the inner Krylov linear solver, which indicates higher computing cost.

5.2. CANTILEVER MICRO-BEAM

The cantilever micro-beam is a classical MEMS device that has been studied extensively [6,7,9,23]. The beam considered in this paper is $500\mu m$ long, $50\mu m$ wide, $14.35\mu m$ thick, fixed with one end and positioned $1\mu m$ above a ground plane, as in Figure 11. When a voltage is applied between the beam and the ground, the electrostatic force is induced due to the charge distribution on the surface of the beam. This electrostatic force causes beam deflection that redistributes the surface charges and as a result, changes the electrostatic force. An equilibrium state will be obtained if the forces due to the beam deflection and the surface charges balance each other. Similar to the MEMS parallel plate capacitor, as the applied voltage increases, the free end of the beam will approach the ground plane and finally touch it at the pull-in voltage.

There is no analytical solution available for this problem; however, the pull-in voltage was estimated by Osterberg *et.al*. [23] as

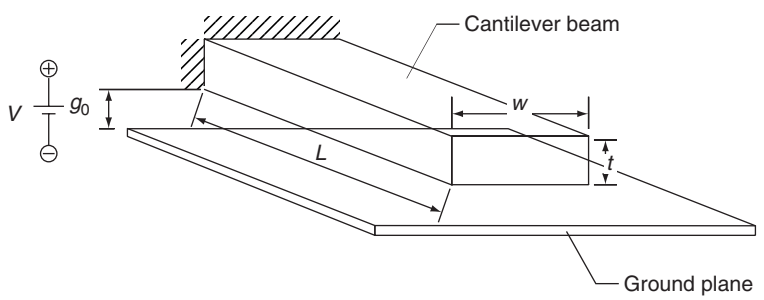

Figure 11 Cantilever micro-beam.

$$V_{PI} = \sqrt{\frac{0.28\tilde{E}t^3 g_0^3}{\varepsilon L^4 \left(1 + 0.42\frac{g_0}{w}\right)}} \tag{35}$$

where t is the beam thickness, g_0 the undeformed gap between the beam and the ground plane, ε the permittivity, L the beam length, w the beam wide and $\tilde{E}$ the effective stiffness which is defined as

$$\tilde{E} = \begin{cases} E & w \le 5t \\ \dfrac{E}{1-\nu^2} & w > 5t \end{cases} \tag{36}$$

where E is Young's modulus and ν the Poisson ratio. For this example, $E = 169GPa$ and $\nu = 0.3$ are used, thus the estimated pull-in voltage is 15.83V according to Eqn.(35).

The beam is discretized into 50 8-node elements for FE analysis, and the ground plane is discretized into 80 4-node elements for BE analysis. Simulations are executed using the four methods for different applied voltages.

The convergence histories of the four methods are shown in Figure 12. At the voltage of 15V, all the four methods exhibit similar convergence characteristics, as in Figure 12(a) and (b). But as shown in Figure 12(c) and (d), if the applied voltage is 15.88V, the staggered/relaxation method achieves convergent until 110 iterations, which is due to the increased coupling between mechanical and electrostatic fields. And other three methods converge rapidly although the quasi-Newton and the RSA both need a little more iterations than the multilevel-Newton method.

Table 2 gives the performances of the four methods. All these methods converge until 15.89V which is very near the theoretical pull-in. For low applied voltages, the staggered/relaxation method is the best choice because it not only requires less or equivalent function evaluations and CPU time but also easy to implement. However, as the applied voltage increases, it converges slower and slower, while the other three methods exhibit better performances. Although in very few high applied voltage cases the RSA scheme needs a little more function evaluations than the quasi-Newton method, the CPU time required by the previous is very close to the latter. This is due to the matrix calculation involved in Broyden update, i.e. Eqn.(16). If finer meshes are adopted, the Broyden updata will cost much more CPU time, which means the RSA scheme is actually more efficient than the quasi-Newton method for this example, and the multilevel Newton has higher computational cost due to function evaluations in the inner Krylov loop.

5.3. CROSS BARS

The cross bars is an example which exhibits extreme nonlinear features, thus it's able to test the robustness of the four methods.

The cross bars are shown in Figure 13 [22]. This example consists of two orthogonal bars with same parameters: the dimension $10\mu m \times 0.5\mu m \times 0.5\mu$m, the Young's modulus $169GPa$ and the Poisson ratio 0.3. Bar B and the far end of bar A are fixed, and the minimum distance between these two bars is $1\mu m$. If a voltage is applied between the two bars, the free end of bar A will bend towards bar B.

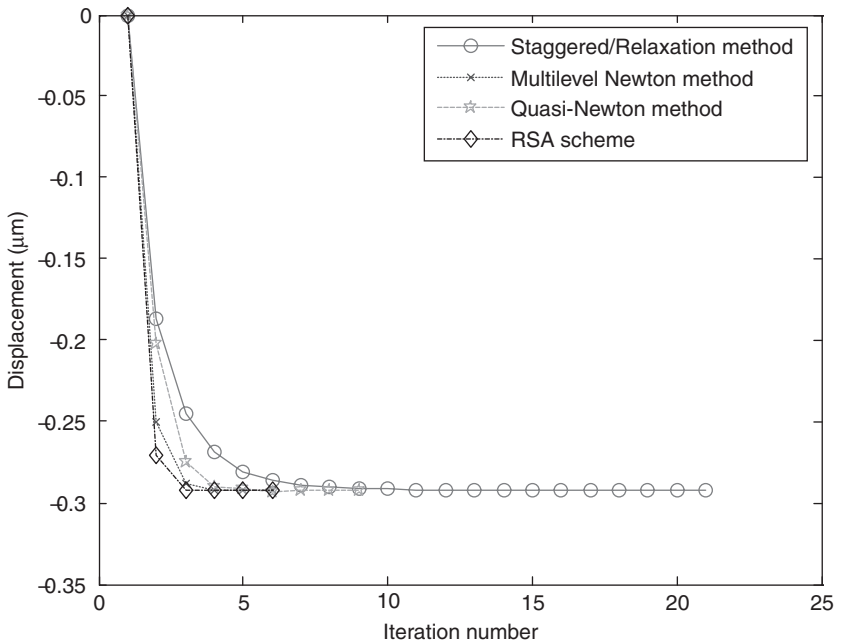

(a) Applied voltage at 15V (global view)

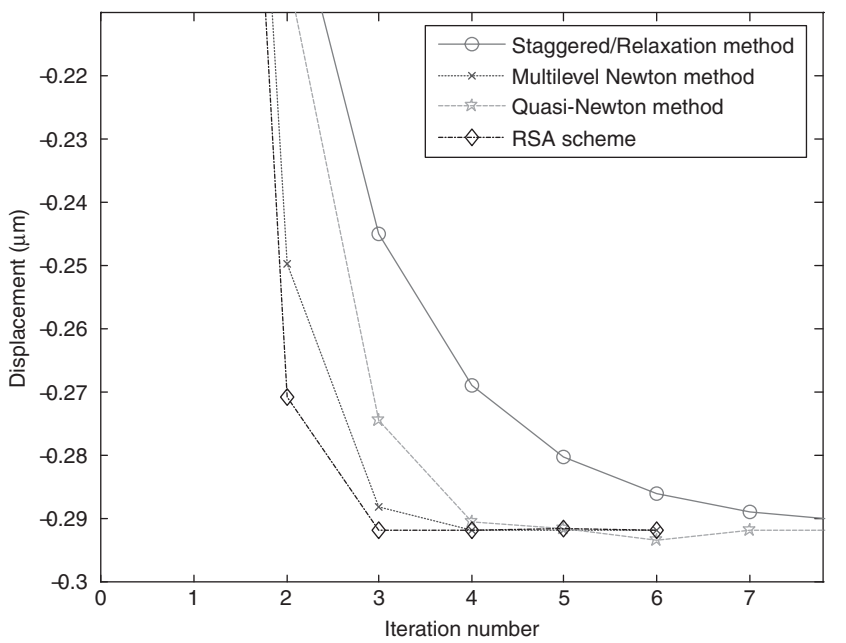

(b) Applied voltage at 15V (local enlargement)

Figure 12 *(Continued).*

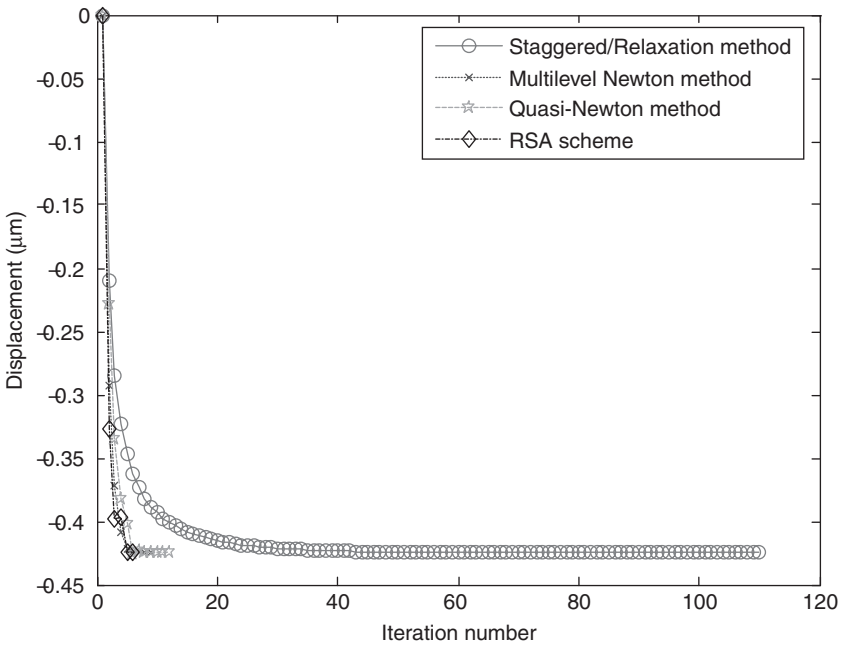

(c) Applied voltage at 15.88V (global view)

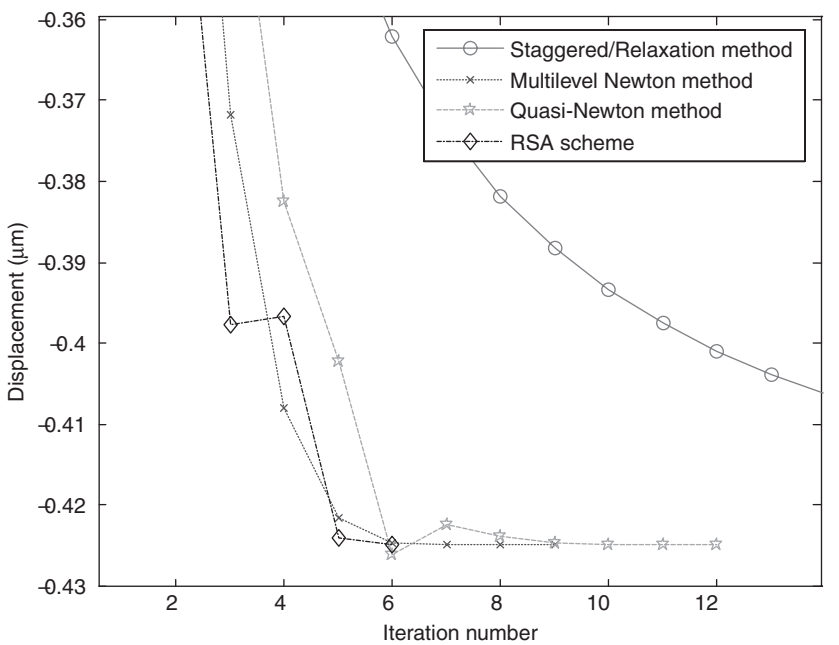

(d) Applied voltage at 15.88V (local enlargement)

Figure 12 Convergence histories for cantilever micro-beam example.

Table 2 Performances for cantilever micro-beam example

Voltage (V)	Function evaluations				CPU time (s)			
	Staggered/ relaxation	Multilevel Newton	Quasi-Newton	RSA	Staggered/ relaxation	Multilevel Newton	Quasi-Newton	RSA
2	4	12	5	6	2	14	9	4
6	6	15	6	6	5	15	10	4
10	9	18	7	6	8	23	12	4
14	15	23	9	8	13	22	15	6
15	21	25	9	12	18	28	16	10
15.5	30	26	11	18	23	26	18	15
15.8	54	29	13	28	39	33	21	23
15.83	63	32	12	32	41	31	20	24
15.85	72	28	12	26	47	35	20	22
15.88	110	30	12	12	61	34	21	9
15.89	Failed	Failed	Failed	Failed	N/A	N/A	N/A	N/A

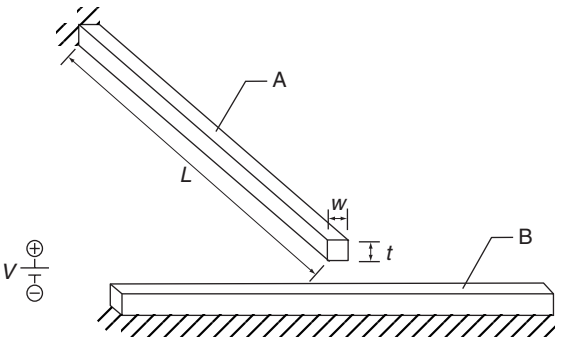

Figure 13 Cross bars.

Bar A is discretized into 20 8-node elements which are used for FE analysis, and bar B is discretized into 80 4-node elements for BE analysis. The convergence histories of the four methods are illustrated in Figure 13. When the applied voltage is 930V, as shown in Figure 14(a) and (b), all methods converge although the staggered/relaxation more slowly. But if the voltage increases, for example, to 1000V as shown in Figure 14(c) and (d), the staggered/relaxation method fails to converge after 200 iterations, and other three methods still work well and converge rapidly.

Table 3 shows the performances of the four methods. Similar with the results of the previous two examples, the staggered/relaxation method requires less function evaluations and CPU time for low applied voltages, while the multilevel Newton method and the RSA scheme are more efficient as the applied voltage increases. It should also be noticed that the quasi-Newton method is not always successful, this is due to the bad initial conditions (here zeros at all nodes) which causes violent changes of the displacements (see Figure 14) and sometimes makes BE solver fail. In order to resolve this matter, voltage stepping technique can be used, e.g. taking the solution obtained at 700V as the initial conditions for 800V. Furthermore, the staggered/relaxation method fails to converge because of the increased coupling and nonlinearity between mechanical and electrostatic fields when the applied voltage is more than 930V, while the RSA scheme still converges at higher voltages, which is also a proof that the latter has looser convergence conditions, as presented in section 4.1.1.

6. CONCLUSIONS

This paper presents the RSA scheme for multiphysics simulation of MEMS. The principle, implementation procedure and convergence condition of this scheme are introduced. Other three conventional coupling algorithms, i.e. the staggered/relaxation, the multilevel Newton and the quasi-Newton methods, are also reviewed. The RSA scheme is then applied on MEMS electrostatic actuators problems. The simulation results show that: 1) the RSA scheme is easy to implement; 2) it is cheaper than the other three methods for the examples illustrated in this paper; 3) it is able to converge even if the staggered/relaxation method fails and; 4) it is not sensitive to the initial conditions.

Although the RSA scheme is promising for MEMS multiphysics simulation, this is only in the context of electrostatic actuator problems. Future work will be done to validate the availability of the RSA scheme to other types of examples, such as fluid-structure interactions or transient problems.

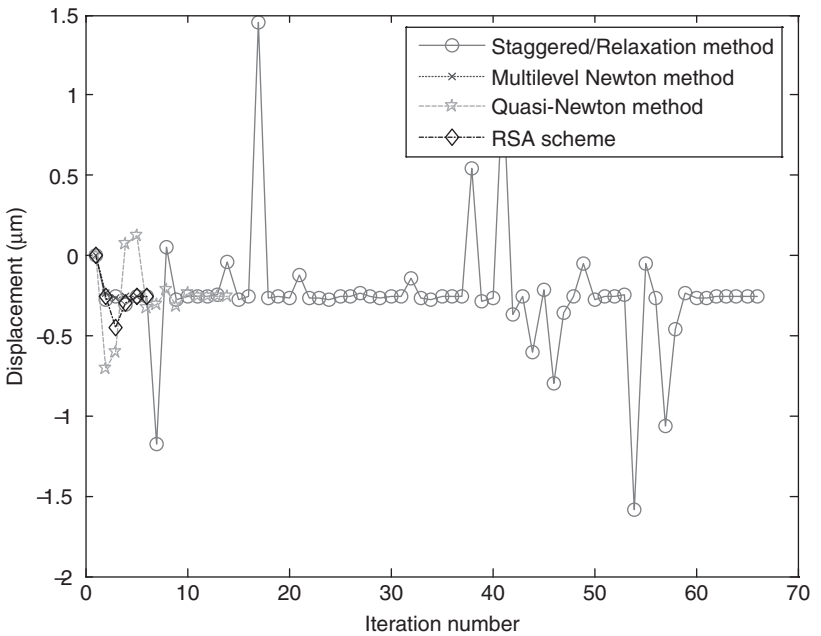

(a) Applied voltage at 930V (global view)

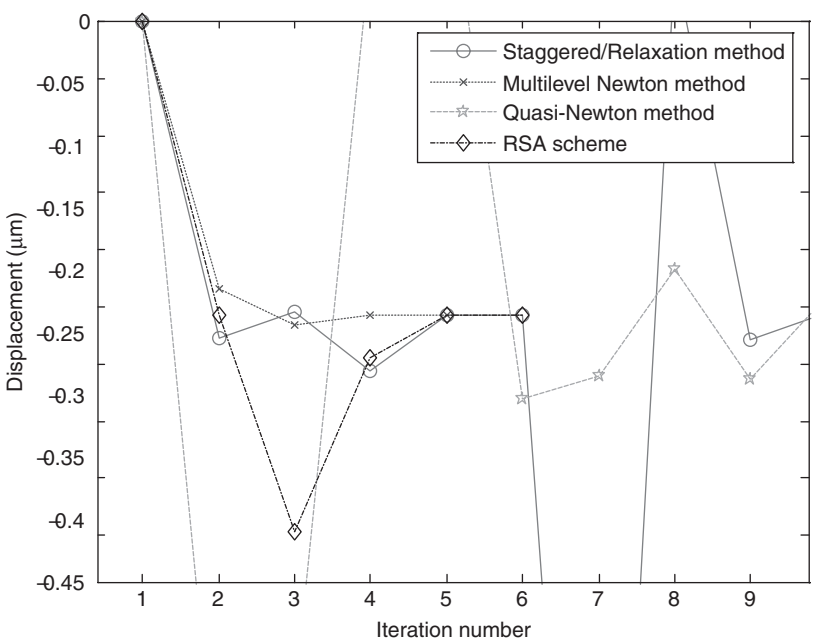

(b) Applied voltage at 930V (local enlargement)

Figure 14 *(Continued).*

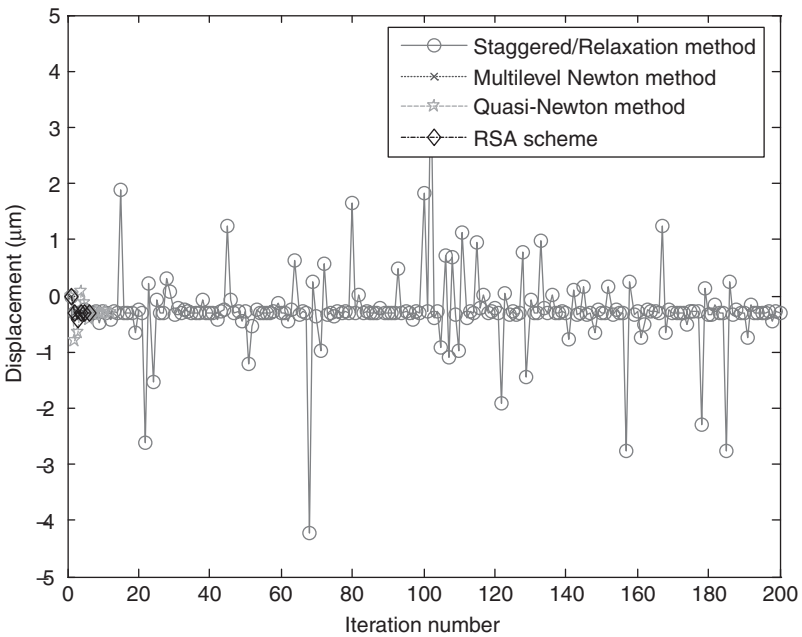

(c) Applied voltage at 1000V (global view)

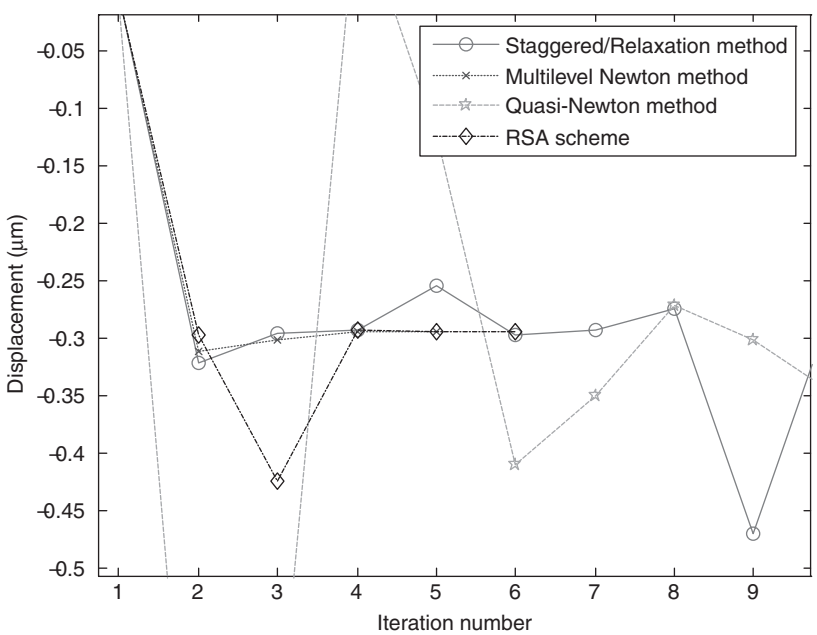

(d) Applied voltage at 1000V (local enlargement)

Figure 14 Convergence histories for cross bars example.

Table 3 Performances for cross bars example

Voltage (V)	Function evaluations				CPU time (s)			
	Staggered/ relaxation	Multilevel Newton	Quasi-Newton	RSA	Staggered/ relaxation	Multilevel Newton	Quasi-Newton	RSA
500	6	13	8	8	4	14	7	5
600	6	15	8	8	4	15	7	5
700	6	18	10	8	5	20	8	5
800	15	16	Failed	24	11	17	N/A	14
900	60	25	Failed	30	31	28	N/A	19
930	66	18	14	12	48	23	11	8
940	Failed	19	Failed	16	N/A	25	N/A	11
1000	Failed	16	12	12	N/A	18	9	8

REFERENCES

[1] Senturia S.D., 1998. "CAD challenges for microsensors, microactuators, and microsystems", *Proceedings of the IEEE*, **86**(8), pp.1611–1626.

[2] COMSOL, 2004. *FEMLAB User's Guide*. COMSOL AB.

[3] ANSYS, 2004. *ANSYS User Manual*. ANSYS, Inc., Canonsburg.

[4] Cai X., Yie H., Osterberg P., et. al., 1993. "A relaxation/multipole-accelerated scheme for self-consistent electromechanical analysis of complex 3-D micromechanical structures", *Proceedings of the 1993 IEEE/ACM International Conference on Computer-Aided-Design*, pp. 283–286.

[5] Senturia S.D., Aluru N.R., White J., 1997. "Simulating the behavior of MEMS devices: Computational methods and needs", *IEEE Computational Sci. & Eng. Magazine*, **4**(1), pp. 30–43.

[6] Yie H., Cai X., White J., 1994. "Convergence properties of relaxation versus the surface-newton generalized-conjugate residual algorithm for self-consistent electromechanical analysis of 3-D micro-electro-mechanical structure", *Proceedings of IEEE NUPAD V*, Honolulu, Hawaii, pp. 137–140.

[7] Aluru N.R., White J., 1999. "A multilevel Newton method for mixed-energy domain simulation of MEMS", *IEEE Journal of Microelectromechanical Systems*, **8**(3), pp. 299–308.

[8] Kelley, C.T., 2003. *Solving Nonlinear Equations with Newton's Method,* Philadelphia, U.S.: Society for Industrial and Applied Mathematics.

[9] Senturia S.D., 2001. *Microsystem Design*, Kluwer Academic Publishers.

[10] Lautrup B., 2005. "The PDE's of Continuum Physics", *Proceedings of the Workshop on PDE methods in Computer Graphics*, Copenhagen, Denmark.

[11] Jin J.M., 1993. *The Finite Element Method in Electromagnetics*. New York: John Wiley & Sons.

[12] ANSYS, 2004. *ANSYS Coupled-Field Analysis Guide*. ANSYS, Inc., Canonsburg.

[13] Hibbit, 2004. *ABAQUS User's Manual*. ABAQUS Inc.

[14] Nabors K., Kim S., et. al., 1992. *FastCap User's Guide*. Massachusetts Institute of Technology, Cambridge.

[15] Rudin W., 1976. *Principles of Mathematical Analysis*. McGraw-Hill.

[16] Mathews J.H., Fink K.D., 2004. *Numerical Methods Using MATLAB, 4th Ed.*, Upper Saddle River, N.J.: Pearson Prentice Hall.

[17] Kelley C.T., 1995. *Iterative Methods for Linear and Nonlinear Equations*, Philadelphia, U.S.: Society for Industrial and Applied Mathematics.

[18] Knoll D.A., Keyes D.E., 2004. "Jacobian-free Newton-Krylov methods: a survey of approaches and applications", *Journal of Computational Physics*, **193**, pp. 357–396.

[19] Shashkin, Y. A., 1991. *Fixed Points*. Providence, RI: Amer. Math. Soc.

[20] Nievergelt Y., 1995. "The condition of Steffensen's acceleration in several variables", *Journal of Computational and Applied Mathematics*, **58**(3), pp. 291–305.

[21] Farhat C., Lesoinne M., et. al., 1998. "Load and motion transfer algorithms for fluid/structure interaction problems with non-matching discrete interfaces: Momentum and energy conservation,optimal discretization and application to aeroelasticity", *Computer Methods in Applied Mechanics and Engineering*, **157**(1–2), pp. 95–114.

[22] Cai X., Osterberg P., Yie H., et. al., 1994. "Self-consistent electromechanical analysis of complex 3-D microelectro-mechanical structures using relaxation/multipole-accelerated method", *Sensors Materials*, **6**(2), pp. 85–99.

[23] Osterberg P.M., Senturia S.D., 1997. "M-TEST: a test chip for MEMS material property measurement using electrostatically actuated test structures", *IEEE Journal of Microelectromechanical Systems*, **6**(2), pp. 107–118.